Enantioselective switch on responses of dissipative chiral molecules

Chong Ye,[1,*] Xiaowei Mu,[1] Yifan Sun,[1] Libin Fu,[2,†] and Xiangdong Zhang[1,‡]
[1]*Beijing Key Laboratory of Nanophotonics and Ultrafine Optoelectronic Systems, School of Physics, Beijing Institute of Technology, 100081 Beijing, China*
[2]*Graduate School of China Academy of Engineering Physics, Beijing 100193, China*

(Received 26 June 2023; revised 8 November 2023; accepted 25 January 2024; published 20 February 2024)

Enantiodetection is an important and challenging task across natural sciences. The cyclic three-level models of chiral molecules provided possibilities to obtain the ultimate limit of the enantioselectivities in purely electric dipole effects, yielding an emerging frontier in enantiodetection. However, the generated enantioselectivities were usually severely reduced in the strong decoherence region, failing most of the related chiroptical methods. Here, we propose enantioselective switches of molecular responses by well designing the electromagnetic fields based on the dissipative cyclic three-level model of chiral molecules and provide a chiroptical method of enantiodetection. In our switches, the steady-state responses are turned on for the selected enantiomer and simultaneously turned off for its mirror image, which corresponds to the ultimate limit of enantioselectivities. The switches can survive in the strong decoherence regions, and so does the suggested chiroptical method of enantiodetection. Our results give more insight into answering whether the enantioselective responses of light based on the cyclic three-level model can survive in the strong decoherence region and thus have a potential impact on further research.

DOI: 10.1103/PhysRevA.109.023114

I. INTRODUCTION

Chiral molecules are ubiquitous. They contain two species, named enantiomers, that are mirror images of each other but are not superimposable by translations and rotations. While two enantiomers share almost identical physical properties, such as melting and boiling points, they play significantly different roles in broad classes of chemical reactions, biological activity, and the function of drugs. Beyond these, there is constant interest in measuring the predicted parity violation (PV) in small chiral molecules due to weak nuclear force [1–5]. Therefore, enantiodetection, aiming to decide enantiomeric excess (i.e., the excess of one enantiomer over the other in a chiral mixture), is an extremely important and challenging task across natural sciences [6–21]. Traditionally, the enantiodetection was accomplished by using optical rotation, circular dichroism, and Raman optical activity [6–9]. The differences between the responses of two enantiomers under the same driving fields result from the interference between electric-dipole and weak magnetic-dipole (or electric-quadrupole) light-matter interactions, making the enantioselectivities (i.e., the relative differences) usually tiny and not freely adjustable.

Nowadays, developing more efficient chiroptical methods purely relying on electric-dipole light-molecule interactions is becoming an emerging frontier. The suggested electric-dipole-based methodologies with strong laser fields included photoelectron circular dichroism (PECD) [22], photoexcitation circular dichroism (PXCD) [14], high harmonic generation (HHG) symmetry-breaking spectroscopy [23,24], and others [25–29] (for more details, see a recent review [30] and the references therein). Yet, the applied fields were usually too strong, resulting in the breaking of molecular structures.

There were also electric-dipole-based methodologies based on cyclic three-level models of chiral molecules introduced by Král *et al.* [31], without the requirement of strong laser fields. The products of the corresponding three electric-dipole transition moments change signs with enantiomers, making molecules of opposite chirality respond differently to the same driving electromagnetic fields. Based on the cyclic three-level model, enantiospecific state transfer (ESST) [31–40], spatial separation of two enantiomers [41–43], enantiodiscrimination [44–50], and enantioconversion [51–56] were theoretically discussed.

ESST is about transferring two enantiomers from the same initial states to two final states of different energies. People are interested in the fast methods of ESST [32–40] because the initial method [31] was based on the slow adiabatic process. The two enantiomers after ESST can be further spatially separated to obtain the enantiopure sample of desired chirality by using energetic processes. The spatial separation of two enantiomers was also discussed by using enantioselective light-induced fields [41–43]. For enantiodiscrimination, different responses of light, such as the enantioselective light absorption [44], the enantioselective three-wave mixing [57], the enantioselective light refraction [45,58], the enantioselective ac Stark effect [46,47], and the enantioselective responses of a hybrid cavity-molecule system [48–50,59], were discussed. It is even possible to convert chiral mixtures to enantiopure samples [51–56] by including achiral electronic or vibrational states in the cyclic three-level model.

*yechong@bit.edu.cn
†lbfu@gscaep.ac.cn
‡zhangxd@bit.edu.cn

On the experimental side, ESST was explored in cold gas-phase samples [60–62] by manipulating rotational transitions of chiral molecules in the microwave band. The working model therein is different from the original model composed of vibrational or electronic transitions [31], where the molecular decoherence, the Doppler effect, and the phase-mismatching cause the enantioselectivities to hardly survive [63]. The cold gas-phase sample manipulated in the microwave band is almost unaffected by these problems and thus provides an ideal platform to develop novel chiroptical methods [33–40,45–47,60–62] and gain a better microscopic understanding of molecular chirality [64]. Another successful example is the enantioselective microwave three-wave mixing for enantiodiscrimination [65–71], where the yielding signals of two enantiomers differ in phase by π.

To extend the applications of the cyclic three-level model of chiral molecules, it is crucial to know whether the enantioselective responses of light based on the cyclic three-level model can survive in large molecular decoherence regions. Unfortunately, the answer is usually negative for most related chiroptical methods. Taking enantioselective ac Stark spectroscopy as an example [46,47], the molecular decoherence gives rise to spectral broadening, which can overwhelm the enantioselectivities in the spectroscopy in the large decoherence region and make the chiroptical method fail. To deal with this problem, the advanced probe method by using frequency-entangled photon pairs [72] and the data-analysis method with the help of machine learning [73] were suggested.

In this paper, we explore the question by examining the steady-state physics of a dissipative cyclic three-level model of chiral molecules with the consideration of bath temperature. Our results show that strong enantioselectivities and even the ultimate limit of enantioselectivities can survive in the large decoherence region. By appropriately designing the three applied electromagnetic fields, we can obtain enantioselective switches of steady-state responses. That is to say, the responses are turned on for the selected enantiomer and simultaneously turned off for its mirror image (i.e., the ultimate limit of enantioselectivities). When the phase of one driving field is increased by 180°, the responses of the two enantiomers exchange with each other, yielding the mirror chiral switch of the initial chiral switch. By comparing the responses in a chiral switch and its mirror switch, we can determine the enantiomeric excess of chiral mixtures.

II. DISSIPATIVE CYCLIC THREE-LEVEL MODEL

To exclude the effect of other problems and make our results experimentally reachable, we still work in the cold gas-phase samples and in the microwave band, where the decoherence rates can be adjusted by increasing the density of the buffer gas. The rotations of chiral molecules are described by asymmetric top rotors, whose eigenfunctions can be denoted as $|J_{\tau,M}\rangle$. Here, J is the angular momentum quantum number, M is the magnetic quantum number, and τ runs from $-J$ to J in unit steps in the order of increasing energy. We choose the working states as $|1\rangle = |0_{0,0}\rangle$, $|2\rangle = |1_{-1,0}\rangle$, and $|3\rangle = |1_{0,1}\rangle$ [74,75]. They are in the electronic and vibrational ground state, such that our proposal works in the microwave region. By denoting the energies of the working states as $\hbar v_j$,

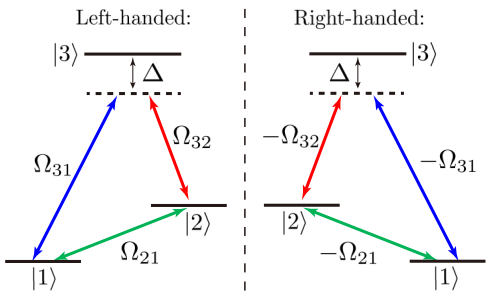

FIG. 1. Model of the left- and right-handed chiral molecules as cyclic three-level systems. Three electromagnetic fields couple to the electric-dipole transitions of two enantiomers in a cyclic manner with different coupling strengths, $\Omega_{lj}^{L} = -\Omega_{lj}^{R} = \Omega_{lj}$ ($3 \geqslant l > j \geqslant 1$).

we give the bare transition angular frequency of the transition $|l\rangle \leftrightarrow |j\rangle$ as $v_{lj} = v_l - v_j$ ($l > j$).

Three electromagnetic fields $\vec{\boldsymbol{E}}_{21} = \vec{\boldsymbol{e}}_z \mathcal{E}_{21} e^{i\omega_{21}t} + \text{c.c.}$, $\vec{\boldsymbol{E}}_{31} = \vec{\boldsymbol{e}}_{+1} \mathcal{E}_{31} e^{i\omega_{31}t} + \text{c.c.}$, and $\vec{\boldsymbol{E}}_{32} = \vec{\boldsymbol{e}}_{+1} \mathcal{E}_{32} e^{i\omega_{32}t} + \text{c.c.}$ with the complex amplitude $\mathcal{E}_{lj}$ are constantly applied to the sample of chiral molecules in the three-photon resonance condition (i.e., $\omega_{31} = \omega_{21} + \omega_{32}$). Here, the polarization vectors are $\vec{\boldsymbol{e}}_{+1} = (\vec{\boldsymbol{e}}_x + i\vec{\boldsymbol{e}}_y)/\sqrt{2}$ and $\vec{\boldsymbol{e}}_{-1} = -(\vec{\boldsymbol{e}}_x - i\vec{\boldsymbol{e}}_y)/\sqrt{2}$. Three applied fields are near-resonantly coupled with the corresponding transitions in a cyclic manner, $|2\rangle \leftrightarrow |1\rangle \leftrightarrow |3\rangle \leftrightarrow |2\rangle$ (see Fig. 1). The other selection-rule-allowed electric-dipole transitions with different bare transition frequencies are off-resonantly coupled with the applied fields and thus are negligible. In this sense, rotational averaging is already involved because the magnetic degenerated states of the working states are not coupled to the working models [74].

For simplicity and without loss of generality, we choose the angular frequencies of the applied electromagnetic fields as $\omega_{21} = v_{21}$ and $\omega_{31} - \omega_{32} = v_{21}$. In the rotation-wave approximation, the Hamiltonians of the two enantiomers in the interaction picture are

$$H_Q = \hbar\Delta|3\rangle\langle 3| + \sum_{l>j=1}^{3} \hbar\Omega_{lj}^{Q}|l\rangle\langle j| + \text{H.c.}, \tag{1}$$

where $Q = (L, R)$ is used to distinguish two enantiomers. The coupling strengths are given by $\Omega_{lj}^{Q} = \vec{\boldsymbol{d}}_{lj}^{Q} \cdot \vec{\boldsymbol{e}}_{lj} \mathcal{E}_{lj}/(2\hbar)$, where $\vec{\boldsymbol{e}}_{lj}$ are unit vectors for the fields. Because transition electric-dipole moments $\vec{\boldsymbol{d}}_{lj}^{Q}$ change sign with enantiomers (i.e., $\vec{\boldsymbol{d}}_{lj}^{L} = -\vec{\boldsymbol{d}}_{lj}^{R} = \vec{\boldsymbol{d}}_{lj}$), the coupling strengths in Eq. (1) are enantioselective,

$$\Omega_{lj}^{L} = -\Omega_{lj}^{R} = \Omega_{lj}. \tag{2}$$

The evolution of dissipative chiral molecules under the driving of Hamiltonian (1) is given by the master equation [76,77]

$$\dot{\rho} = -i[H_Q, \rho] + \mathcal{L}(\rho). \tag{3}$$

To consider the dissipation of chiral molecules, we have introduced the superoperator $\mathcal{L}(\rho) = \mathcal{L}_{\text{rel}}^{\text{in}}(\rho) + \mathcal{L}_{\text{rel}}^{\text{exc}}$

$(\rho)+\mathcal{L}_{\rm dep}(\rho)$. It is due to the effect of the environment-system coupling under the Markovian approximation [77].

In the standard Lindblad approach, we have [76]

$$\mathcal{L}^{\rm in}_{\rm rel}(\rho)=-\sum_{l>j=1}^{3}\Big[\bar{n}^{\rm b}_{lj}\frac{\Gamma_{lj}}{2}(\sigma_{jl}\sigma_{lj}\rho-\sigma_{lj}\rho\sigma_{jl}) + \big(\bar{n}^{\rm b}_{lj}+1\big)\frac{\Gamma_{lj}}{2}(\sigma_{lj}\sigma_{jl}\rho-\sigma_{jl}\rho\sigma_{lj})\Big]+{\rm H.c.}, \quad (4)$$

where we have used $\sigma_{lj}=|l\rangle\langle j|$ and Γ_{lj} are relaxation rates. The subscript "rel" is the abbreviation for "relaxation." It indicates the source of the dissipation that the system and environment exchange energy, making the change of both the diagonal and off-diagonal terms of the density matrices. This is usually due to the coupling of the system with the thermal vacuum (e.g., spontaneous emissions) and inelastic collisions. The subscript "in" indicates the relaxation that happens among the working states of the cyclic three-level model. The bath temperature is considered by using *nonzero* thermal average boson number,

$$\bar{n}^{\rm b}_{lj}=\frac{1}{\exp\left(\frac{\hbar v_{lj}}{k_BT}\right)-1}, \quad (5)$$

where k_B, T, and v_{lj} are the Boltzmann constant, the bath temperature, and the angular frequency of the bath boson, respectively.

When the term of $\mathcal{L}^{\rm in}_{\rm rel}$ is active, the population transits between states of the three-level model. The chiral molecules can emit energy to or absorb energy from the buffer gases, i.e., the chiral molecules can be excited from a lower-energy state to a higher-energy state or deexcited due to the collisions with the buffer gases. Then, the equilibrium state in the absence of electromagnetic fields is the thermal state. This is consistent with the existing buffer-gas-cooling experiments [65–71], where all three working levels are populated almost equally. In contrast, in the previous dissipative model [46,47], the chiral molecules can only emit energy to the buffer gases, and thus the equilibrium state in the absence of electromagnetic fields is the ground state.

The superoperator $\mathcal{L}^{\rm exc}_{\rm rel}(\rho)$ mimics the spontaneous emissions and inelastic collisions concerning other states outside the working model. When the term of $\mathcal{L}^{\rm exc}_{\rm rel}$ is active, the population transits between states in and out of the three-level model. These processes are accompanied by changes in the off-diagonal terms. In the appearance of the relaxation including the states outside the working states, the three-level model cannot fully describe real chiral molecules. However, we note that the dynamic equilibrium between the working levels and others does exist. Therefore, we mimic the decoherence of the cyclic three-level model due to the states outside the working model as

$$\begin{aligned}\big[\mathcal{L}^{\rm exc}_{\rm rel}(\rho)\big]_{jj}&=-\gamma^{\rm exc}_{j}\big(\rho_{jj}-\rho^{\rm ES}_{jj}\big),\\ \big[\mathcal{L}^{\rm exc}_{\rm rel}(\rho)\big]_{lj}&=-\gamma^{\rm exc}_{lj}\rho_{lj},\end{aligned} \quad (6)$$

where $\rho^{\rm ES}_{jj}$ is the population of the state $|j\rangle$ in the field-free thermal equilibrium state of real chiral molecules. $\gamma^{\rm exc}_{j}$ and $\gamma^{\rm exc}_{lj}$ are the corresponding decoherence rates related to the diagonal and off-diagonal terms of the density matrices.

The pure dephasing due to elastic collisions is described by $\mathcal{L}_{\rm dep}(\rho)$ with

$$[\mathcal{L}_{\rm dep}(\rho)]_{lj}=-\gamma^{\rm ph}_{lj}\rho_{lj},\quad [\mathcal{L}_{\rm dep}(\rho)]_{jj}=0. \quad (7)$$

In elastic collisions, the system does not exchange energy with the environment. Thus, when the term of $\mathcal{L}_{\rm dep}$ is active, only the off-diagonal terms of the density matrices are changed without affecting the diagonal terms. This type of dissipation is known as pure dephasing. Here, the subscript "dep" is the abbreviation for "dephasing" and $\gamma^{\rm ph}_{lj}$ are the dephasing rates.

III. CHIRAL SWITCH OF STEADY-STATE RESPONSES

The state of the system in dynamic equilibrium is usually called the steady state, which can be given by solving the following steady-state equation:

$$0=-i[H_Q,\rho]+\mathcal{L}(\rho). \quad (8)$$

Here, we focus on ρ_{21}, which governs the response of a single steady-state molecule concerning the induced polarization $\vec{\boldsymbol{P}}(\omega_{21})=\vec{\boldsymbol{e}}_zP_z(\omega_{21})\propto\rho_{21}$. By further designing Ω_{21}, we expect to obtain chiral switches of two types of molecular responses with $\rho_{21}=0$ and ${\rm Im}(\rho_{21})=0$ for a selected enantiomer.

We assume the sample takes the typical geometry of the buffer-gas cell [65] of $10\times10\times10$ cm^3. The size of the molecular sample is much smaller than the typical wavelengths of microwave electromagnetic fields. Therefore, the molecules at different positions are approximately phase matched. Further, we choose the waists of the Gaussian beams to be much larger than the size of the sample, such that the coupling strengths are approximately spatially uniform in the interaction region. By taking the typical buffer-gas-cooling experimental values [65–71], we use $\Omega_{32}=\Omega_{31}=\bar{\Omega}=2\pi\times1$ MHz for simplicity and without loss of generality.

In typical buffer-gas-cooling experiments [65–71], the rotational state coherence is destroyed on a timescale of about 6 microseconds. The estimated decoherence rate is about $2\pi\times1/6\simeq2\pi\times0.1$ MHz, which corresponds to the weak-decoherence case. In the studies of transient physics [65–71], such a decoherence rate is negligible. But, in our study of steady-state physics, the decoherence rate should not be neglected. We demonstrate the chiral switch of steady-state responses with an example of 1,2-propanediol. The corresponding bare transition angular frequencies are $v_{21}=2\pi\times6431.06$ MHz, $v_{32}=2\pi\times4931.95$ MHz, and $v_{31}=2\pi\times11363.01$ MHz [78]. By taking the typical buffer-gas-cooling temperature of 10 K, we estimate that $\rho^{\rm ES}_{11}\simeq1‰$, $\rho^{\rm ES}_{22}\simeq0.9696‰$, and $\rho^{\rm ES}_{33}\simeq0.9431‰$ [78].

A. Switch of radiations

The first type of chiral response of our interest is the induced radiation of the angular frequency ω_{21} at far-field point $\vec{\boldsymbol{r}}=r\vec{\boldsymbol{e}}_x$, which is given as [46]

$$\vec{\boldsymbol{E}}\simeq\frac{k^2_{21}}{4\pi\varepsilon_0}\frac{e^{ik_{21}r}}{r^3}[\vec{\boldsymbol{r}}\times n\mathcal{V}\rho_{21}\vec{\boldsymbol{d}}_{21}]\times\vec{\boldsymbol{r}}. \quad (9)$$

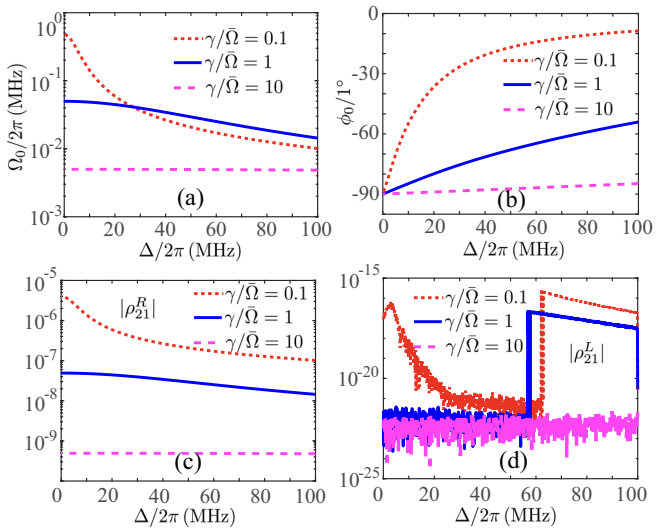

FIG. 2. Chiral switch of radiations. (a) and (b) give Ω_0 and ϕ_0 as functions of the detuning at different decoherence rates. (c) and (d) give the corresponding $|\rho_{21}^R|$ and $|\rho_{21}^L|$. We choose $\Omega_{32} = \Omega_{31} = \bar{\Omega} = 2\pi \times 1$ MHz for simulations.

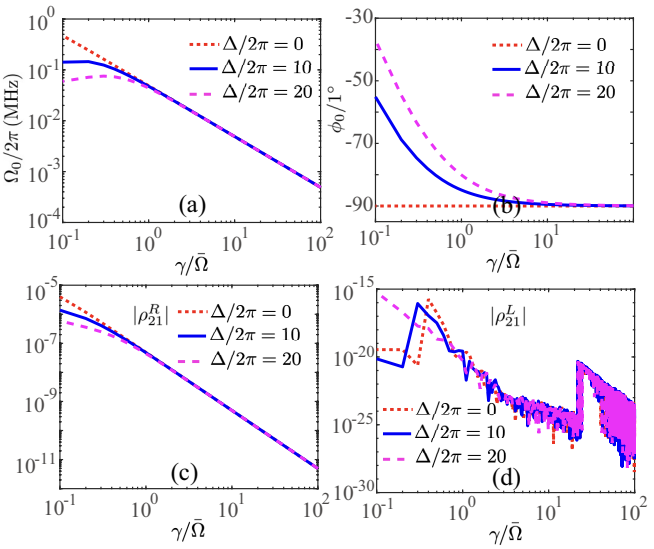

FIG. 3. Chiral switch of radiations. (a) and (b) give Ω_0 and ϕ_0 as functions of $\gamma/\bar{\Omega}$ at different values of detuning Δ. (c) and (d) give the corresponding $|\rho_{21}^R|$ and $|\rho_{21}^L|$. We choose $\Omega_{32} = \Omega_{31} = \bar{\Omega} = 2\pi \times 1$ MHz for simulations.

Here, we assume the sample is placed at the origin. The density of the sample is denoted as n. The volume of the sample is denoted as $\mathcal{V}$. We are interested in the case $\rho_{21}^L = 0$ and $\rho_{21}^R \neq 0$. This condition can be satisfied by adjusting the complex coupling strength Ω_{21}. In such a case, the corresponding amplitude and phase of Ω_{21} is denoted as Ω_0 and ϕ_0, which are given by solving Eq. (8) of the left-handed molecule with the condition of $\rho_{21}^L = 0$. We note that when changing the phase of Ω_{32} by π, the behaviors of two enantiomers will exchange with each other. That is to say, in the case of Ω_0 and $\phi_0 + 180^\circ$, we can obtain a new switch with $\rho_{21}^L \neq 0$ and $\rho_{21}^R = 0$, which is the mirror switch of the initial one with Ω_0 and ϕ_0.

In Figs. 2(a) and 2(b), we give Ω_0 and ϕ_0 as functions of the detuning at weak- (red dotted lines), medium- (blue solid lines), and strong- (magenta dashed lines) decoherence rates. Here, for simplicity and without loss of generality, we have assumed $\Gamma_{lj} = \gamma_{lj}^{\rm ph} + \gamma_{lj}^{\rm exc} = \gamma_j^{\rm exc} = \gamma$. To further confirm the switch of radiation, we inset Ω_0 and ϕ_0 back to Eq. (8) of the two enantiomers and solve the corresponding ρ_{21}^R and ρ_{21}^L. Because of numerical error, ρ_{21}^L are *nonzero* [see Fig. 2(d)]. But ρ_{21}^L are sufficiently small and are about 10 orders of magnitude smaller than the corresponding ρ_{21}^R [Fig. 2(c)]. Further, in Figs. 3(a)–3(d), we give Ω_0 and ϕ_0 as functions of $\gamma/\bar{\Omega}$ for different values of detuning as well as the corresponding values of $|\rho_{21}^R|$ and $|\rho_{21}^L|$. These results demonstrate that the chiral switch of radiations is a universal phenomenon of dissipative chiral molecules driven in the cyclic three-level model, which even survives at strong decoherence region with $\gamma/\bar{\Omega} \geqslant 10$.

The induced radiation $\vec{E}$ and the driving field $\vec{E}_{21}$ have the same frequency, such that they cannot be distinguished in the frequency domain. To solve this problem, we can detect the free-induced decay signals after suddenly turning off all the driving fields after the system enters the steady state. At the weak decoherence $\gamma/\bar{\Omega} = 0.1$ (or, equivalently, $\gamma = 2\pi \times 0.1$ MHz) and $\Delta = 0$, we have that the signal at $r = 1$ m for enantiopure right-handed molecules is about $|\vec{E}| \simeq 4.5 \times 10^{-6}$ V/m by using the typical density of the 1,2-propanediol sample in the buffer-gas cell [65] ($n = 10^{12}$ cm^{-3}). We note that it is possible to detect such weak microwave radiations by using microwave single-photon detectors [79,80].

B. Switch of absorptions

The second type of chiral response of our interest is the absorption of the driving field $\vec{E}_{21}$. In the slowly varying amplitude and phase approximation, it is given as

$$\delta E \simeq -nl\frac{k_{21}}{\varepsilon_0}\mathrm{Im}(\rho_{21})d_{21}, \tag{10}$$

where n is the density of the sample and l is the propagating length of E_{21} in the sample. The switches of radiations are also switches of absorptions. At the weak decoherence $\gamma/\bar{\Omega} = 0.1$ (or, equivalently, $\gamma = 0.1$ MHz) and $\Delta = 0$, we have $\mathrm{Im}(\rho_{21}^L) = -8.277 \times 10^{-7}$ for the enantiopure sample. Therefore, the absorption signal of the enantiopure sample is about $\delta E \simeq 2.88 \times 10^{-6}$ V/m, where we use the typical density and length of the 1,2-propanediol sample in the buffer-gas cell [65] with $n = 10^{12}$ cm^{-3} and $l = 10$ cm.

We note that for the switches of absorptions, the requirement on the steady state is $\mathrm{Im}(\rho_{21}) = 0$ for one enantiomer and $\mathrm{Im}(\rho_{21}) \neq 0$ for its mirror image. That is to say, the switches of absorptions may not be switches of radiations. In Fig. 4(a), we show Ω_0 for the switch of absorptions at different ϕ. The corresponding $\mathrm{Im}(\rho_{21})$ for the two enantiomers are given in Fig. 4(b). These results show that only the absorptions of one enantiomer are *nonzero*, i.e., the switches of absorptions. We can see that the switches of absorptions for one enantiomer change to the switches for its mirror image via increasing the phase by 180°, i.e., the switches of absorptions have their mirror chiral switches. We can see there are two exceptional points near $\phi \simeq 90^\circ$ and $\phi \simeq 270^\circ$,

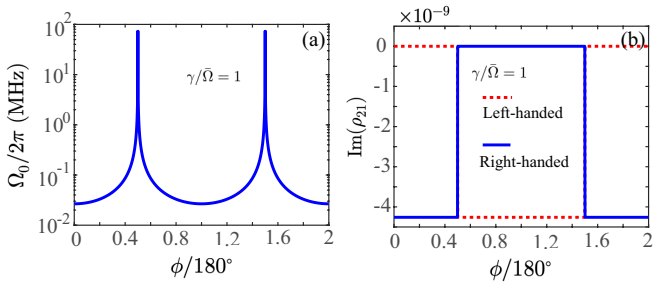

FIG. 4. Chiral switches of absorptions. (a) gives Ω_0 for the switch of absorptions at different ϕ. (b) gives the corresponding $\mathrm{Im}(\rho_{21})$ for the two enantiomers. We choose $\Omega_{32}=\Omega_{31}=\bar{\Omega}=2\pi\times 1$ MHz for simulations.

where the absorptions of the two enantiomers are turned off simultaneously.

Similar to the switches of radiations, the appearance of switches of absorptions is a universal property of dissipative chiral molecules driven in the cyclic three-level model. To demonstrate this, we give Ω_0 as a function of Δ for $\phi=0$ in the small-decoherence case with $\gamma/\bar{\Omega}=0.1$, the medium-decoherence case with $\gamma/\bar{\Omega}=1$, and the large-decoherence case with $\gamma/\bar{\Omega}=10$ [see Fig. 5(a)]. The corresponding

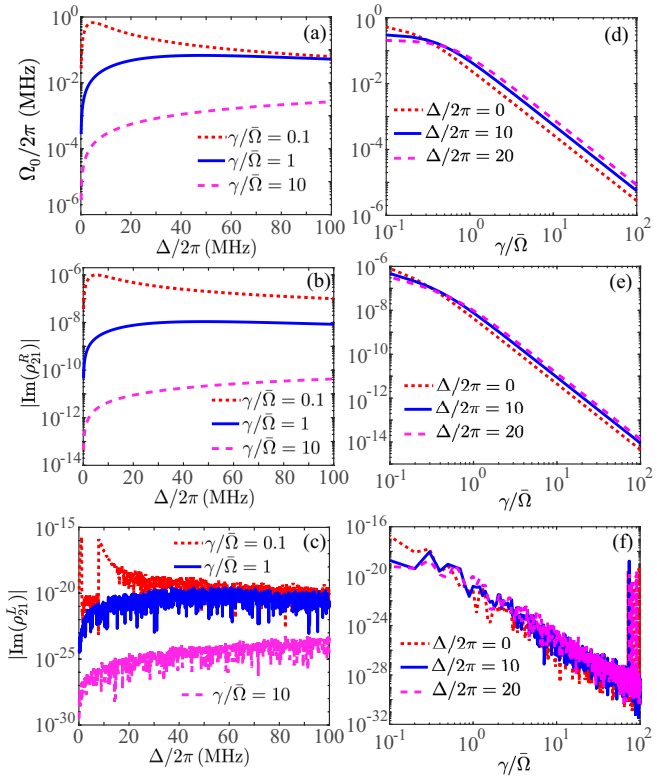

FIG. 5. Chiral switches of absorptions. (a) gives Ω_0 as a function of Δ for $\phi=0$ in the small-decoherence case with $\gamma/\bar{\Omega}=0.1$, the medium-decoherence case with $\gamma/\bar{\Omega}=1$, and the large-decoherence case with $\gamma/\bar{\Omega}=10$. (b) and (c) give the corresponding $|\mathrm{Im}(\rho_{21})|$ of the two enantiomers. (d) gives Ω_0 as a function of $\gamma/\bar{\Omega}$ for different Δ. (e) and (f) give the corresponding $|\mathrm{Im}(\rho_{21})|$ of the two enantiomers. We choose $\Omega_{32}=\Omega_{31}=\bar{\Omega}=2\pi\times 1$ MHz for simulations.

$|\mathrm{Im}(\rho_{21})|$ of the two enantiomers are given in Figs. 5(b) and 5(c). Because of numerical error, $|\mathrm{Im}(\rho_{21}^L)|$ are *nonzero*. But they are sufficiently small and are about 10 orders of magnitude smaller than the corresponding $\mathrm{Im}(\rho_{21}^R)$. At $\Delta=0$, we find that $\mathrm{Im}(\rho_{21}^R)\simeq\mathrm{Im}(\rho_{21}^L)\simeq 0$, which are exceptional points. We also give Ω_0 as a function of $\gamma/\bar{\Omega}$ for different Δ in Fig. 5(d). The corresponding steady state $|\mathrm{Im}(\rho_{21})|$ for two enantiomers is given in Figs. 5(e) and 5(f). The results in Figs. 5(d)–5(f) further confirm the universality of the appearance of the switches.

As we have shown, the enantioselective switches are obtained by appropriately designing the driven fields. Although the steady state is the result of decoherence processes, the high enantioselectivities in the signals are the results of the enantioselective cyclic three-level Hamiltonian (1). In the process of obtaining well-designed driving fields for the case of induced radiation, we have inserted $\rho_{12}^L=0$ in Eq. (8) and use Ω_{12} as the unknown parameter. Then, we obtain equations concerning Ω_{12} and other unknown parameters of the density matrix. The equations are solvable because they are linear and the number of unknowns is equal to the number of equations. Under the same fields, we usually have $\rho_{12}^R\neq 0$ because the Hamiltonians of two enantiomers are different. In the process of obtaining well-designed driving fields for the case of induced radiation, we insert $\mathrm{Im}[\rho_{12}^L]=0$ in Eq. (8) and use Ω_{12} as the unknown parameter. Then, we can fix the phase or amplitude of Ω_{12} to find the solutions. In this case, the number of unknowns is equal to the number of equations. Under the same fields, we usually have $\mathrm{Im}[\rho_{12}^R]\neq 0$. These are the underlying mathematics of our enantioselective switches, which are preserved without regard to concrete forms of the dissipative model and thus make it possible to obtain high enantioselectivities in the strong-decoherence regions. We note that due to the enantioselective cyclic three-level Hamiltonian (1), the diagonal terms ρ_{ii} are also enantioselective in the steady state.

IV. DETECTION OF ENANTIOMERIC EXCESS

Using the chiral switches, we can determine the enantiomeric excess of a chiral mixture [$\varepsilon\equiv 2(p_L-p_R)/(p_L+p_R)$]. Here, p_L and p_R are the proportions of left- and right-handed molecules in the chiral mixture. For this purpose, we use the fact that the steady-state density matrix of one enantiomer is the same as that of the enantiomer of opposite chirality by increasing the phase ϕ by 180°, i.e., $\rho^L(\phi)=\rho^R(\phi+180°)$. Because the electric dipoles change signs with two enantiomers (i.e., $\vec{d}_{21}^{\,L}=-\vec{d}_{21}^{\,R}$), the collected signals of chiral mixtures in the two cases are [see Fig. 4(a)]

$$S_1=S_Lp_L+S_Rp_R,\quad S_2=-S_Rp_L-S_Lp_R, \tag{11}$$

where S_L and S_R are the corresponding signals for enantiopure samples of opposite chiralities. When the applied fields are well designed to form the chiral switches, we have $S_L=0$ and $S_R\neq 0$, such that the enantiomeric excess is estimated as

$$\varepsilon_e=2\frac{S_2+S_1}{S_2-S_1}. \tag{12}$$

Because $Q(=L,R)$ does not indicate the absolute configuration of the chiral molecule, the enantiomeric excess here is

not the absolute enantiomeric excess concerning the absolute configuration.

The advantages of our scheme are as follows. Our scheme can serve as a sensitive chiroptical method in and beyond the weak-decoherence regions because of the universality of the chiral switches. In contrast, other spectroscopic methods [46,47] based on the cyclic three-level model are only efficient in the weak-decoherence region. Our scheme is sensitive to rotational constants and thus is applicable for mixtures of different types of chiral molecules. Our scheme yields *nonzero* signals in racemic samples. This is impossible in the three-wave mixing spectroscopy [57,65–71]. When the details of the dissipative model of chiral molecules [i.e., $\mathcal{L}(\rho)$] are well known, the switches can be obtained, as shown in Sec. III, such that the current chiroptical method can be used determine the enantiomeric excess without the requirement of enantiopure samples. In contrast, in the three-wave mixing spectroscopy [57,65–71] and the traditional chiroptical methods [6–9], the enantiopure samples are required. When the details of the dissipative model of chiral molecules are unknown, the switches can be obtained by using an enantiopure sample as a reference to find the appropriate applied fields. The searching task for the switch of absorptions is a single-parameter search problem. This offers it an advantage over the switch of radiations whose searching task is a double-parameter search problem.

It is helpful to explore the system error due to the derivations from the perfect chiral switches. In such cases, we have $S_L \neq 0$ and $S_R \neq 0$. According to Eqs. (11) and (12), the relative error due to the derivations is given as

$$\eta \equiv \left|\frac{\varepsilon_e - \varepsilon}{\varepsilon_e + \varepsilon}\right| = \left|\frac{S_L}{S_R}\right|. \tag{13}$$

The relative error is identical for all values of ε and thus serves as a good criterion for our further discussions. In Fig. 6(b), we show the values of η on the $\delta\Omega/\Omega_0 - \delta\phi$ plane for the switches of radiations in the case of $\gamma/\bar{\Omega} = 0.1$ and $\Delta = 0$. Highly efficient estimation of enantiomeric excess with relative error of less than 1% can be obtained in the red dashed cycle. Further, we give the critical value $\delta\Omega_c$ for $\eta = 1\%$ at $\delta\phi = 0$ [see Fig. 6(c)] and the critical value $\delta\phi_c$ for $\eta = 1\%$ at $\delta\Omega = 0$ [see Fig. 6(d)] as the functions of Δ at different $\gamma/\bar{\Omega}$. In Fig. 6(e), we give the values of η as a function of $\delta\Omega$ for the switches of absorptions at $\gamma/\bar{\Omega} = 0.1$, $\Delta = 2\pi \times 10$ MHz, and $\phi = 0$. In Fig. 6(f), we give the critical values $\delta\Omega_c$ for $\eta = 1\%$ as the functions of Δ at $\phi = 0$ at different $\gamma/\bar{\Omega}$. These results indicate that our scheme should be implemented in the systems in which the precise controls of the coupling strengths have been realized [60–62,65–71].

V. CONCLUSIONS

In summary, we have shown two types of enantioselective switches on responses of the dissipative chiral molecules driven in the cyclic three-level model in the weak-decoherence region and beyond. Based on these, we also have suggested a scheme to determine the enantiomeric excess. In our scheme,

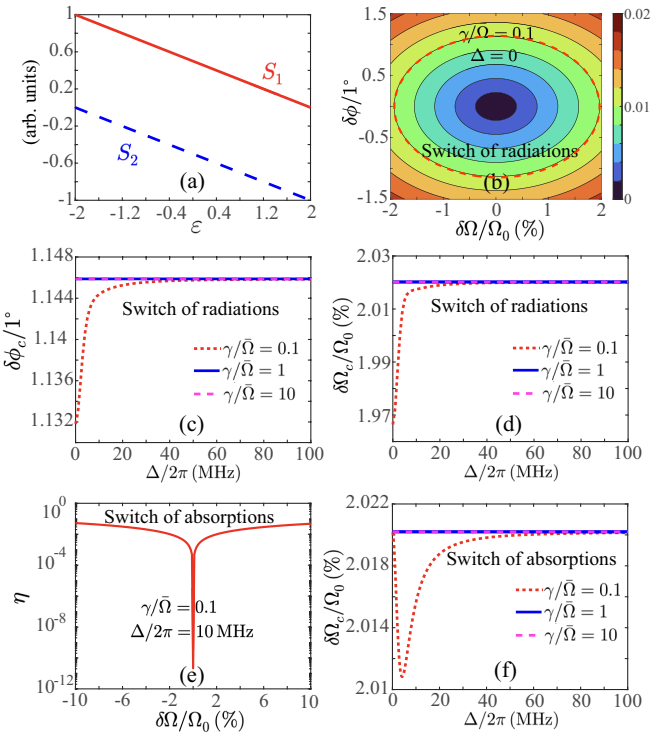

FIG. 6. Detection of enantiomeric excess. (a) gives the signals in the chiral switch and its mirror chiral switch as the functions of enantiomeric excess. (b)–(d) explore the relative error for the switches of radiations. (b) gives the relative error η in the $\delta\Omega/\Omega_0 - \delta\phi$ plane. The red dashed cycle indicates the relative error of 1%. (c) and (d) give the critical values $\delta\Omega_c$ for $\eta = 1\%$ at $\delta\phi = 0$ and $\delta\phi_c$ for $\eta = 1\%$ at $\delta\Omega = 0$ as the functions of Δ at different γ. (e) and (f) explore the relative error for the switches of absorption. (e) gives the values of η as a function of $\delta\Omega$ at $\gamma/\bar{\Omega} = 0.1$, $\Delta = 2\pi \times 10$ MHz, and $\phi = 0$. (f) gives the critical values $\delta\Omega_c$ for $\eta = 1\%$ as the functions of Δ at $\phi = 0$ at different γ.

the enantioselectivities can reach the ultimate limit of 200%, which means the corresponding chiroptical method can be more sensitive than the traditional ones, such as optical rotation, circular dichroism, and Raman optical activity [6–9]. The ultimate limit of enantioselectivities in our switches can survive in and beyond the weak-decoherence region, and so does our scheme of enantiodetection. This offers our scheme an important advantage over other proposals based on the cyclic three-level model of chiral molecules. Although there is still a long way to go for industrial applications, our results do give more insight into answering whether the enantioselective responses of light based on the cyclic three-level model can survive in large molecular decoherence regions and thus have a potential impact on further works.

ACKNOWLEDGMENTS

This work is supported by the National Natural Science Foundation of China (Grants No. 12105011, No. 91850205, No. 11725417, No. 12088101, and No. 11904022).

[1] M. Quack, Molecular parity violation and chirality: the asymmetry of life and the symmetry violations in physics, in *Quantum Systems in Chemistry and Physics: Progress in Methods and Applications* edited by K. Nishikawa, J. Maruani, E. J. Brädas, G. Delgado-Barrio, and P. Piecuch (Dordrecht Springer, Netherlands, 2012), pp. 47–76.

[2] S. Albert, I. Bolotova, Z. Chen, C. Fábri, M. Quack, G. Seyfang, and D. Zindel, Phys. Chem. Chem. Phys. **19**, 11738 (2017).

[3] J. Eills, J. W. Blanchard, L. Bougas, M. G. Kozlov, A. Pines, and D. Budker, Phys. Rev. A **96**, 042119 (2017).

[4] A. Cournol, M. Manceau, M. Pierens, L. Lecordier, D. Tran, R. Santagata, B. Argence, A. Goncharov, O. Lopez, M. Abgrall *et al.*, Quantum Electron. **49**, 288 (2019).

[5] A. Landau, Eduardus, D. Behar, E. R. Wallach, L. F. Pašteka, S. Faraji, A. Borschevsky, and Y. Shagam, J. Chem. Phys. **159**, 114307 (2023).

[6] N. Berova, K. Nakanishi, and R. W. Woody, *Circular Dichroism: Principles and Applications* (Wiley, New York, 2000).

[7] L. D. Barron, *Molecular Light Scattering and Optical Activity* (Cambridge University Press, Cambridge, 2009).

[8] K. W. Busch and M. A. Busch, *Chiral Analysis* (Elsevier, Amsterdam, 2011).

[9] L. A. Nafie, *Vibrational Optical Activity: Principles and Applications* (Wiley, New York, 2011).

[10] H. Rhee, Y.-G. June, J.-S. Lee, K.-K. Lee, J.-H. Ha, Z. H. Kim, S.-J. Jeon, and M. Cho, Nature (London) **458**, 310 (2009).

[11] M. Pitzer, M. Kunitski, A. S. Johnson, T. Jahnke, H. Sann, F. Sturm, L. P. H. Schmidt, H. Schmidt-Böcking, R. Dörner, J. Stohner *et al.*, Science **341**, 1096 (2013).

[12] R. Cireasa, A. Boguslavskiy, B. Pons, M. Wong, D. Descamps, S. Petit, H. Ruf, N. Thiré, A. Ferré, J. Suarez *et al.*, Nat. Phys. **11**, 654 (2015).

[13] S. Beaulieu, A. Comby, A. Clergerie, J. Caillat, D. Descamps, N. Dudovich, B. Fabre, R. Géneaux, F. Légaré, S. Petit *et al.*, Science **358**, 1288 (2017).

[14] S. Beaulieu, A. Comby, D. Descamps, B. Fabre, G. Garcia, R. Géneaux, A. Harvey, F. Légaré, Z. Mašín, L. Nahon *et al.*, Nat. Phys. **14**, 484 (2018).

[15] S. Arnaboldi, G. Salinas, A. Karajić, P. Garrigue, T. Benincori, G. Bonetti, R. Cirilli, S. Bichon, S. Gounel, N. Mano *et al.*, Nat. Chem. **13**, 1241 (2021).

[16] Y. Tang and A. E. Cohen, Phys. Rev. Lett. **104**, 163901 (2010).

[17] Y. Tang and A. E. Cohen, Science **332**, 333 (2011).

[18] T. Wu, W. Zhang, H. Zhang, S. Hou, G. Chen, R. Liu, C. Lu, J. Li, R. Wang, P. Duan *et al.*, Phys. Rev. Lett. **124**, 083901 (2020).

[19] K. A. Forbes and D. L. Andrews, Opt. Lett. **43**, 435 (2018).

[20] K. A. Forbes, Phys. Rev. Lett. **122**, 103201 (2019).

[21] A. Salam and W. Meath, Chem. Phys. **228**, 115 (1998).

[22] E. Bloch, S. Larroque, S. Rozen, S. Beaulieu, A. Comby, S. Beauvarlet, D. Descamps, B. Fabre, S. Petit, R. Taïeb *et al.*, Phys. Rev. X **11**, 041056 (2021).

[23] D. Ayuso, O. Neufeld, A. F. Ordonez, P. Decleva, G. Lerner, O. Cohen, M. Ivanov, and O. Smirnova, Nat. Photon. **13**, 866 (2019).

[24] O. Neufeld, D. Ayuso, P. Decleva, M. Y. Ivanov, O. Smirnova, and O. Cohen, Phys. Rev. X **9**, 031002 (2019).

[25] O. Neufeld, H. Hübener, A. Rubio, and U. De Giovannini, Phys. Rev. Res. **3**, L032006 (2021).

[26] O. Neufeld, O. Wengrowicz, O. Peleg, A. Rubio, and O. Cohen, Opt. Express **30**, 3729 (2021).

[27] D. Ayuso, A. F. Ordonez, M. Ivanov, and O. Smirnova, Optica **8**, 1243 (2021).

[28] D. Ayuso, A. F. Ordonez, P. Decleva, M. Ivanov, and O. Smirnova, Nat. Commun. **12**, 3951 (2021).

[29] D. Ayuso, Phys. Chem. Chem. Phys. **24**, 10193 (2022).

[30] D. Ayuso, A. F. Ordonez, and O. Smirnova, Phys. Chem. Chem. Phys. **24**, 26962 (2022).

[31] P. Král and M. Shapiro, Phys. Rev. Lett. **87**, 183002 (2001).

[32] Y. Li and C. Bruder, Phys. Rev. A **77**, 015403 (2008).

[33] N. V. Vitanov and M. Drewsen, Phys. Rev. Lett. **122**, 173202 (2019).

[34] C. Ye, Q. Zhang, Y.-Y. Chen, and Y. Li, Phys. Rev. A **100**, 043403 (2019).

[35] J.-L. Wu, Y. Wang, J. Song, Y. Xia, S.-L. Su, and Y.-Y. Jiang, Phys. Rev. A **100**, 043413 (2019).

[36] J.-L. Wu, Y. Wang, J.-X. Han, C. Wang, S.-L. Su, Y. Xia, Y. Jiang, and J. Song, Phys. Rev. Appl. **13**, 044021 (2020).

[37] B. T. Torosov, M. Drewsen, and N. V. Vitanov, Phys. Rev. A **101**, 063401 (2020).

[38] B. T. Torosov, M. Drewsen, and N. V. Vitanov, Phys. Rev. Res. **2**, 043235 (2020).

[39] B. Liu, C. Ye, C. P. Sun, and Y. Li, Phys. Rev. A **105**, 043110 (2022).

[40] M. Leibscher, E. Pozzoli, C. Pérez, M. Schnell, M. Sigalotti, U. Boscain, and C. P. Koch, Commun. Phys. **5**, 110 (2022).

[41] Y. Li, C. Bruder, and C. P. Sun, Phys. Rev. Lett. **99**, 130403 (2007).

[42] X. Li and M. Shapiro, J. Chem. Phys. **132**, 194315 (2010).

[43] B. Liu, C. Ye, C. P. Sun, and Y. Li, Phys. Rev. A **104**, 013113 (2021).

[44] W. Z. Jia and L. F. Wei, Phys. Rev. A **84**, 053849 (2011).

[45] Y.-Y. Chen, C. Ye, Q. Zhang, and Y. Li, J. Chem. Phys. **152**, 204305 (2020).

[46] C. Ye, Q. Zhang, Y.-Y. Chen, and Y. Li, Phys. Rev. A **100**, 033411 (2019).

[47] M. R. Cai, C. Ye, H. Dong, and Y. Li, Phys. Rev. Lett. **129**, 103201 (2022).

[48] Y.-H. Kang, Z.-C. Shi, J. Song, and Y. Xia, Opt. Lett. **45**, 4952 (2020).

[49] Y.-Y. Chen, J.-J. Cheng, C. Ye, and Y. Li, Phys. Rev. Res. **4**, 013100 (2022).

[50] Y.-Y. Chen, C. Ye, and Y. Li, Opt. Express **29**, 36132 (2021).

[51] P. Král, I. Thanopulos, M. Shapiro, and D. Cohen, Phys. Rev. Lett. **90**, 033001 (2003).

[52] M. Shapiro, E. Frishman, and P. Brumer, Phys. Rev. Lett. **84**, 1669 (2000).

[53] P. Brumer, E. Frishman, and M. Shapiro, Phys. Rev. A **65**, 015401 (2001).

[54] D. Gerbasi, M. Shapiro, and P. Brumer, J. Chem. Phys. **115**, 5349 (2001).

[55] C. Ye, Q. Zhang, Y.-Y. Chen, and Y. Li, Phys. Rev. Res. **2**, 033064 (2020).

[56] C. Ye, B. Liu, Y.-Y. Chen, and Y. Li, Phys. Rev. A **103**, 022830 (2021).

[57] E. Hirota, Proc. Jpn Acad. B **88**, 120 (2012).

[58] M. Khokhlova, E. Pisanty, S. Patchkovskii, O. Smirnova, and M. Ivanov, Sci. Adv. **8**, eabq1962 (2022).

[59] C. Ye, Y. Sun, Y. Li, and X. Zhang, J. Phys. Chem. Lett. **14**, 6772 (2023).
[60] S. Eibenberger, J. Doyle, and D. Patterson, Phys. Rev. Lett. **118**, 123002 (2017).
[61] C. Pérez, A. L. Steber, S. R. Domingos, A. Krin, D. Schmitz, and M. Schnell, Angew. Chem., Intl. Ed. **56**, 12512 (2017).
[62] J. H. Lee, J. Bischoff, A. O. Hernandez-Castillo, B. Sartakov, G. Meijer, and S. Eibenberger-Arias, Phys. Rev. Lett. **128**, 173001 (2022).
[63] P. Fischer, D. S. Wiersma, R. Righini, B. Champagne, and A. D. Buckingham, Phys. Rev. Lett. **85**, 4253 (2000).
[64] W. Sun, D. S. Tikhonov, H. Singh, A. L. Steber, C. Pérez, and M. Schnell, Nat. Commun. **14**, 934 (2023).
[65] D. Patterson, M. Schnell, and J. M. Doyle, Nature (London) **497**, 475 (2013).
[66] D. Patterson and J. M. Doyle, Phys. Rev. Lett. **111**, 023008 (2013).
[67] D. Patterson and M. Schnell, Phys. Chem. Chem. Phys. **16**, 11114 (2014).
[68] V. A. Shubert, D. Schmitz, D. Patterson, J. M. Doyle, and M. Schnell, Angew. Chem., Intl. Ed. **53**, 1152 (2014).
[69] V. A. Shubert, D. Schmitz, C. Medcraft, A. Krin, D. Patterson, J. M. Doyle, and M. Schnell, J. Chem. Phys. **142**, 214201 (2015).
[70] S. Lobsiger, C. Pérez, L. Evangelisti, K. K. Lehmann, and B. H. Pate, J. Phys. Chem. Lett. **6**, 196 (2015).
[71] V. A. Shubert, D. Schmitz, C. Pérez, C. Medcraft, A. Krin, S. R. Domingos, D. Patterson, and M. Schnell, J. Phys. Chem. Lett. **7**, 341 (2016).
[72] C. Ye, Y. Sun, and X. Zhang, J. Phys. Chem. Lett. **12**, 8591 (2021).
[73] X. Mu, C. Ye, and X. Zhang, J. Phys. Chem. Lett. **14**, 10067 (2023).
[74] C. Ye, Q. Zhang, and Y. Li, Phys. Rev. A **98**, 063401 (2018).
[75] M. Leibscher, T. F. Giesen, and C. P. Koch, J. Chem. Phys. **151**, 014302 (2019).
[76] M. O. Scully and M. S. Zubairy, *Quantum Optics* (Cambridge University Press, New York, 2008).
[77] H.-P. Breuer and F. Petruccione, *The Theory of Open Quantum Systems* (Oxford University Press, New York, 2002).
[78] Q. Zhang, Y.-Y. Chen, C. Ye, and Y. Li, J. Phys. B: At., Mol. Opt. Phys. **53**, 235103 (2020).
[79] K. Inomata, Z. Lin, K. Koshino, W. D. Oliver, J.-S. Tsai, T. Yamamoto, and Y. Nakamura, Nat. Commun. **7**, 12303 (2016).
[80] Z. Wang, Z. Bao, Y. Li, Y. Wu, W. Cai, W. Wang, X. Han, J. Wang, Y. Song, L. Sun *et al.*, Nat. Commun. **13**, 6104 (2022).